Spatio-temporal Coordinated Restoration for Multi-voltage-level Power Systems During Wind Storms

Changming Chen, Yunchu Wang, Shunjiang Yu, Bing Chen, *Senior Member*, *IEEE*, Zikang Shen, Ze Li, Hongtao Wang, *Senior Member*, *IEEE*, and Zhenzhi Lin, *Senior Member*, *IEEE*

***Abstract*—Among disasters that may lead to large-scale blackouts of power systems, wind storms introduce spatio-temporal variations in restoration security risks, making large-scale power system restoration more difficult. Power system restoration during wind storms requires coordinated efforts among the regional independent system operators, transmission system operators, and distribution system operators. However, existing research mainly focuses on the coordination between transmission system operators and distribution system operators, which limits its applicability to large-scale blackouts caused by wind storms. Therefore, a spatio-temporal coordinated restoration method based on restoration security risk assessment for multi-voltage-level power systems (MVLPSs) is proposed in this paper. Typhoons, known for their high wind speeds and destructive power, are considered as the disaster scenario. First, a spatio-temporal restoration security risk assessment approach is proposed to reduce additional control costs caused by restoration security risks. Then, a spatio-temporal coordinated restoration framework for MVLPSs is established, and a triple-level optimization model for the spatio-temporal coordinated restoration of MVLPSs is proposed to maximize the net restoration benefits of MVLPSs during the full-stage restoration process. Finally, case studies on an actual 379-bus MVLPS in China are conducted to verify that the proposed method can achieve higher net restoration benefits compared with existing restoration methods.**

***Index Terms*—Power system, blackout, spatio-temporal coordinated restoration, restoration security risk, wind storm.**

I. Introduction

OVER the past few years, power systems have faced severe threats from extreme wind storm disasters. For example, Hurricane Irma left about 3.8 million customers without power in Florida, USA, in 2017. In 2021, Typhoon In-Fa caused a large-scale power outage in China, disrupting transportation and power systems and affecting 4.1 million people. In the same year, Typhoon Chanthu struck the eastern coast of China, leading to widespread power outages in Fujian and Zhejiang provinces. More recently, in 2022, Typhoon Noru caused significant power outages in the Philippines, impacting millions of people and critical infrastructure [1]. Therefore, it is crucial to develop appropriate power system restoration strategies following wind storm disasters to effectively mitigate negative impacts on the general public and economy [2].

The restoration problem of power systems after large-scale blackouts caused by wind storm disasters has characteristics such as multiple stages, multiple dispatching levels, and high restoration security risks [3]. In terms of multi-stage restoration, existing research has explored black-start, network reconfiguration, and load restoration. Specifically, research on black-start can be mainly categorized into three categories: zoning and parallel black-start [4], extended black-start [5], and coordinated black-start in transmission and distribution systems [6]. Current research on network reconfiguration mainly focuses on skeleton network configuration [7] and optimizing restoration paths [8]. For load restoration, the primary objective is to accelerate the restoration process and reduce economic losses in the transmission network [9], distribution network [10], and coupled transmission and distribution networks [11]. Although these three stages have different characteristics and objectives, their boundaries are sometimes unclear, making it difficult to develop independent yet well-coordinated restoration strategies. In this context, some studies have explored coordinated multi-stage restoration strategies for power systems [12]. For instance, in [13], power system restoration models that simultaneously consider the black-start and network reconfiguration stages are proposed. In [14], a bi-level coordinated entire-stage restoration model is proposed for the power system considering the support of various flexible resources, which can expedite the restoration process and maximize the

Manuscript received: January 12, 2025; revised: April 6, 2025; accepted: June 7, 2025. Date of CrossCheck: June 7, 2025. Date of online publication: June 27, 2025.

This work was supported by the National Natural Science Foundation of China (No. 52077195) and the Science and Technology Projects of State Grid Corporation of China (No. 5100-202240015A-1-1-ZN).

C. Chen is with the College of Electrical Engineering and Automation, Fuzhou University, Fuzhou 350108, China (e-mail: chenchangming@fzu.edu.cn).

Y. Wang, S. Yu, Z. Shen, and Z. Lin (corresponding author) are with the College of Electrical Engineering, Zhejiang University, Hangzhou 310027, China (e-mail: wangyunchu_ee@zju.edu.cn; yushunjiang@zju.edu.cn; 22210014@zju.edu.cn; linzhenzhi@zju.edu.cn).

B. Chen is with the Electric Power Research Institute State Grid Jiangsu Electric Power Co., Ltd., Nanjing 211100, China (e-mail: cbsure@163.com).

Z. Li is with the State Grid Electric Power Research Institute (NARI Group Corporation), Nanjing 210003, China (e-mail: lize3@sgepri.sgcc.com.cn).

H. Wang is with the College of Electrical Engineering, Shandong University, Jinan 250100, China (e-mail: whtwhm@sdu.edu.cn).

DOI: 10.35833/MPCE.2025.000034

recoverable load. In terms of coordinated restoration at multiple dispatching levels, existing research primarily focuses on the coordinated restoration of the transmission system operator (TSO) and distribution system operator (DSO). For instance, in [6], a distributed black-start optimization method for transmission and distribution systems is proposed to minimize blackout costs and improve restoration efficiency. In [15], a decentralized restoration model to achieve efficient and coordinated load restoration in coupled transmission and distribution systems is established. In [16], a two-stage predictive control approach is proposed to enable effective dynamic load restoration decisions in coupled transmission and distribution systems with renewable energy sources. In [11], a load restoration optimization model for a wind-power-integrated system with multiple transmission and distribution systems is proposed. To address restoration security risks, some studies utilize uncertainty handling methods such as the conditional value at risk (CVaR) method [11], model predictive control theory [17], stochastic programming [18], and robust optimization [19] to deal with various uncertainties during the restoration process. Besides, some studies incorporate security risk metrics to quantify and monetize restoration security risks and include them in the objective function [20].

The aforementioned studies have made significant contributions to the development of power system restoration techniques. However, there are still some shortcomings in existing research.

1) There is a lack of in-depth exploration into the impacts of restoration security risks on power system restoration during typhoon disasters, particularly from both temporal and spatial perspectives. More specifically, the typhoon is one of the wind storm types with the highest wind speed and strongest destructive power, and higher wind speeds during a typhoon correspond to higher restoration security risks, which can lead to line restoration failures and increased control costs. Besides, the dynamic nature of typhoon paths and wind speeds results in varying restoration security risks for different transmission lines at the same time step, as well as for the same transmission line at different time steps. Therefore, traditional power system restoration methods are not suitable for large-scale power outages during typhoon disasters, and it is necessary to develop a spatio-temporal restoration security risk assessment approach for power system restoration during typhoon disasters.

2) There is a lack of research on the spatio-temporal coordinated restoration method for multi-voltage-level power systems (MVLPSs). In China, power system operators are generally divided into national independent system operator, regional independent system operator (R-ISO), TSO, and DSO according to the voltage levels. In scenarios of extensive power outages caused by typhoon disasters, such as state-level blackouts, the involved dispatching organizations include not only TSOs and DSOs but also higher-level R-ISOs. In the temporal dimension, different dispatching organizations have distinct restoration targets during various periods of power system restoration. The TSO needs to consider strategies for black-start, network reconfiguration, and load restoration, while R-ISO does not consider load restoration, and DSO does not consider the black-start. In the spatial dimension, power systems of different voltage levels are interconnected through coupling buses, enabling power exchange during the restoration process. Specifically, R-ISO provides black-start power to TSO, while TSO assists in restoring the network of R-ISO. Similarly, TSO supplies power to DSO, which in turn aligns its load restoration with the requirements of TSO. Hence, there is an urgent need to investigate the spatio-temporal coordinated restoration for MVLPSs to enhance restoration speed and net benefits in scenarios of extensive power outages.

To this end, this paper proposes a restoration security risk assessment based spatio-temporal coordinated restoration method during wind storms for MVLPSs to address the aforementioned issues. The contributions of this paper are summarized as follows.

1) A spatio-temporal restoration security risk assessment approach for MVLPSs is proposed, which is based on Miyazaki-Masao, Rankine, and series-parallel system reliability assessment theories. The proposed approach can accurately evaluate the restoration security risks of power systems at different locations and time points under typhoon disasters, thus reducing additional control costs caused by the restoration security risks.

2) A spatio-temporal coordinated restoration framework for MVLPSs considering the restoration security risk assessment is established, which combines the spatial coordination of R-ISO, TSO, and DSO, and the temporal coordination from the initial stage of extensive power outages to the completion of load restoration, thereby enhancing the net benefits of power system restoration.

3) A restoration security risk assessment based triple-level optimization model for the spatio-temporal coordinated restoration of MVLPSs is proposed. First, evaluation indexes for net restoration benefits considering restoration security risks are established. Then, three restoration optimization submodels are developed for the R-ISO, TSO, and DSO, respectively, to maximize their net restoration benefits. The proposed model effectively coordinates the full-stage restoration process of MVLPSs in both temporal and spatial dimensions, which achieves faster black-start, network reconfiguration, and load restoration speeds, leading to higher net restoration benefits compared with existing restoration models.

The rest of this paper is organized as follows: Section II introduces the spatio-temporal coordinated restoration framework for MVLPSs considering the restoration security risk assessment. Section III establishes a restoration security risk assessment based triple-level optimization model for the coordinated restoration of MVLPSs. Case studies and corresponding conclusions are presented in Sections IV and V, respectively.

II. Spatio-temporal Coordinated Restoration Framework for MVLPSs Considering Restoration Security Risk Assessment

A. Spatio-temporal Restoration Security Risk Assessment Approach for MVLPSs

During a typhoon disaster, the restoration reliability of

transmission lines is related to the typhoon wind speed. The distances between the transmission lines and the typhoon center change as the typhoon moves. Therefore, the wind speeds of the same transmission line at different time steps or of different transmission lines at the same time step are different, resulting in different line restoration reliabilities [21]. Lower line restoration reliability leads to higher restoration security risks, which vary over time and space as the typhoon moves. Neglecting spatio-temporal restoration security risks when formulating restoration strategies may result in line restoration failures, leading to additional costs [22]. The influence of spatio-temporal restoration security risks on power system restoration strategies in different typhoon scenarios is analyzed in Supplementary Material A Fig. SA1. In Fig. SA1, bus A is restored at time step t, with all three typhoon scenarios passing from the southeast direction. At time step $t+1$ in Scenario 1, line A-D is restored at time step $t+1$ considering the target of restoring generators as soon as possible. Due to that the wind speed and associated restoration security risk of line A-B are much higher than those of line A-D, line A-B remains unrestored at time step $t+1$. At time step $t+2$ in Scenario 1, the typhoon has moved to the northwest, allowing further restoration of both lines A-B and A-D. Similarly, at time step $t+1$ in Scenario 2, both lines A-B and C-D are in the high wind speed area, indicating higher restoration security risks. Therefore, these lines are not restored until the time step $t+2$. In Scenario 3, the typhoon does not pass through these lines, so all four lines are fully restored by the time step $t+2$.

In conclusion, under typhoon disasters, it is necessary to formulate corresponding restoration strategies based on the spatio-temporal variations of restoration security risks to avoid incurring additional costs. Hence, a spatio-temporal restoration security risk assessment approach for MVLPSs based on Miyazaki-Masao, Rankine, and series-parallel system reliability assessment theories is proposed in this paper.

First, the Miyazaki-Masao model is used to obtain the scalar values of translational wind speeds, as represented by (1) and (2), which represents the translational wind component caused by the movement of typhoon. Meanwhile, the Rankine model is applied to calculate the scalar value of circulation wind speeds, as expressed in (3), which describes the rotational wind field around the typhoon center. These two models are widely used in meteorological studies to construct a realistic typhoon wind field, capturing both translational and circulatory wind effects, which directly influence power system restoration security risks [23].

$$v_{l,t}^{\mathrm{tra}} = v_{0,t}^{\mathrm{typ}} \exp[-\pi r_{0,l,t}^{\mathrm{typ}}/(10R_{\max,t}^{\mathrm{typ}})] \tag{1}$$

$$\begin{aligned} r_{0,l,t}^{\mathrm{typ}} = R^{\mathrm{E}} \arccos(&\sin(y_{0,t}^{\mathrm{typ}})\sin(y_{l,t}) + \\ &\cos(y_{0,t}^{\mathrm{typ}})\cos(y_{l,t})\cos(x_{0,t}^{\mathrm{typ}} - x_{l,t})) \end{aligned} \tag{2}$$

$$v_{l,t}^{\mathrm{cir}} = \begin{cases} (r_{0,l,t}^{\mathrm{typ}}/R_{\max,t}^{\mathrm{typ}})V_{\max,t}^{\mathrm{typ}} & r_{0,l,t}^{\mathrm{typ}} \in [0, R_{\max,t}^{\mathrm{typ}}) \\ (R_{\max,t}^{\mathrm{typ}}/r_{0,l,t}^{\mathrm{typ}})V_{\max,t}^{\mathrm{typ}} & r_{0,l,t}^{\mathrm{typ}} \in [R_{\max,t}^{\mathrm{typ}}, \infty) \end{cases} \tag{3}$$

where $v_{l,t}^{\mathrm{tra}}$ and $v_{l,t}^{\mathrm{cir}}$ are the translational and circulation wind speeds of line l at time step t, respectively; $v_{0,t}^{\mathrm{typ}}$ is the translational wind speed of the typhoon center at time step t; $r_{0,l,t}^{\mathrm{typ}}$ is the distance between the typhoon center and line l at time step t; $R_{\max,t}^{\mathrm{typ}}$ and $V_{\max,t}^{\mathrm{typ}}$ are the maximum wind circle radius and wind speed of the typhoon at time step t, respectively; R^{E} is the average radius of the Earth; and $(x_{0,t}^{\mathrm{typ}}, y_{0,t}^{\mathrm{typ}})$ and $(x_{l,t}, y_{l,t})$ are the latitude and longitude coordinates of the typhoon center and line l at time step t, respectively. Note that $x_{l,t}$ and $y_{l,t}$ are the average values of the latitude and longitude coordinates of the initial, middle, and end buses of line l, respectively.

Then, by considering the vector sum of translational and circulation wind speeds and incorporating the influence of terrain on wind speed at the line location, the spatio-temporal wind speed vector is formulated in (4). This comprehensive wind field model provides a more accurate representation of the wind speeds affecting transmission lines, which is essential for evaluating restoration feasibility under typhoon conditions.

$$\boldsymbol{v}_{l,t} = k_l(\boldsymbol{v}_{l,t}^{\mathrm{tra}} + \boldsymbol{v}_{l,t}^{\mathrm{cir}}) \tag{4}$$

where $\boldsymbol{v}_{l,t}$ is the spatio-temporal wind speed vector of line l at time step t; k_l is the terrain correction coefficient for line l; and $\boldsymbol{v}_{l,t}^{\mathrm{tra}}$ and $\boldsymbol{v}_{l,t}^{\mathrm{cir}}$ are the vectors of translational and circulation wind speeds, respectively.

Since transmission lines typically consist of multiple towers, their restoration reliability should account for structural dependencies. Based on the series-parallel system reliability assessment theory [24], we define the restoration reliability index of line l at time step t, i.e., $R_{l,t}$, which is represented by (5). It quantifies the probabilistic impact of extreme wind speeds on restoration success rates, ensuring that restoration decisions consider potential risks and avoid secondary failures caused by premature restoration.

$$R_{l,t} = (\mathrm{e}^{-\gamma_{l,t}^{\mathrm{tow}}/(1-\gamma_{l,t}^{\mathrm{tow}})})^{N_l^{\mathrm{tow}}} \tag{5}$$

where N_l^{tow} is the number of towers of line l; and $\gamma_{l,t}^{\mathrm{tow}}$ is the tower damage probability of line l, which is related to the calculated wind speed $v_{l,t}$ obtained from (4) and can be expressed as:

$$\gamma_{l,t}^{\mathrm{tow}} = \begin{cases} 0 & 0 \le v_{l,t} < v_l^{\mathrm{des}} \\ \mathrm{e}^{a_l(v_{l,t} - 2v_l^{\mathrm{des}})} & v_l^{\mathrm{des}} \le v_{l,t} < 2v_l^{\mathrm{des}} \\ 1 & v_{l,t} \ge 2v_l^{\mathrm{des}} \end{cases} \tag{6}$$

where v_l^{des} is the designed wind speed of line l; and a_l is the tower damage coefficient of line l.

Based on this, the restoration security risk of the power system at time step t, i.e., $f_{\mathrm{RSR},t}$, is defined as:

$$f_{\mathrm{RSR},t} = \sum_{l=1}^{N_{\mathrm{line}}} c_{\mathrm{RSR},l,t} B_{\mathrm{line},l,t} (1 - R_{l,t}) \tag{7}$$

where $B_{\mathrm{line},l,t}$ is the restoration status of line l, with a value of 1 indicating that it is restored; $c_{\mathrm{RSR},l,t}$ is the unit control cost caused by restoration security risk for line l at time step t; and N_{line} is the total number of lines.

B. Spatio-temporal Coordinated Restoration Framework for MVLPSs Considering Restoration Security Risk Assessment

When a state-level blackout occurs, it involves power systems across voltage levels of 500 kV, 220 kV, 110 kV, and below. It should be noted that the coordinated restoration of transmission and distribution networks was studied in our previous work [21]. Building on that foundation, this paper

focuses on the restoration optimization strategy for 110 kV and above power systems, assuming that once 110 kV substations are restored, 110 kV subnetworks and loads recover according to predefined distribution protocols. Therefore, power system restoration below 110 kV is not explicitly considered in this study.

Power systems at different voltage levels are managed and operated by different dispatching centers. It is commonly recognized that the R-ISO, TSO, and DSO manage the 500 kV, 220 kV, and 110 kV power systems, respectively. Traditional two-level restoration models often simplify the transmission network as a single entity, without distinguishing between the distinct jurisdictional responsibilities of R-ISO and TSO. However, in practical large-scale blackouts, restoration decisions at different voltage levels should be optimized separately while maintaining inter-operator coordination. In this context, this paper proposes a spatio-temporal coordinated restoration framework for MVLPSs considering the restoration security risk assessment, as illustrated in Fig. 1.

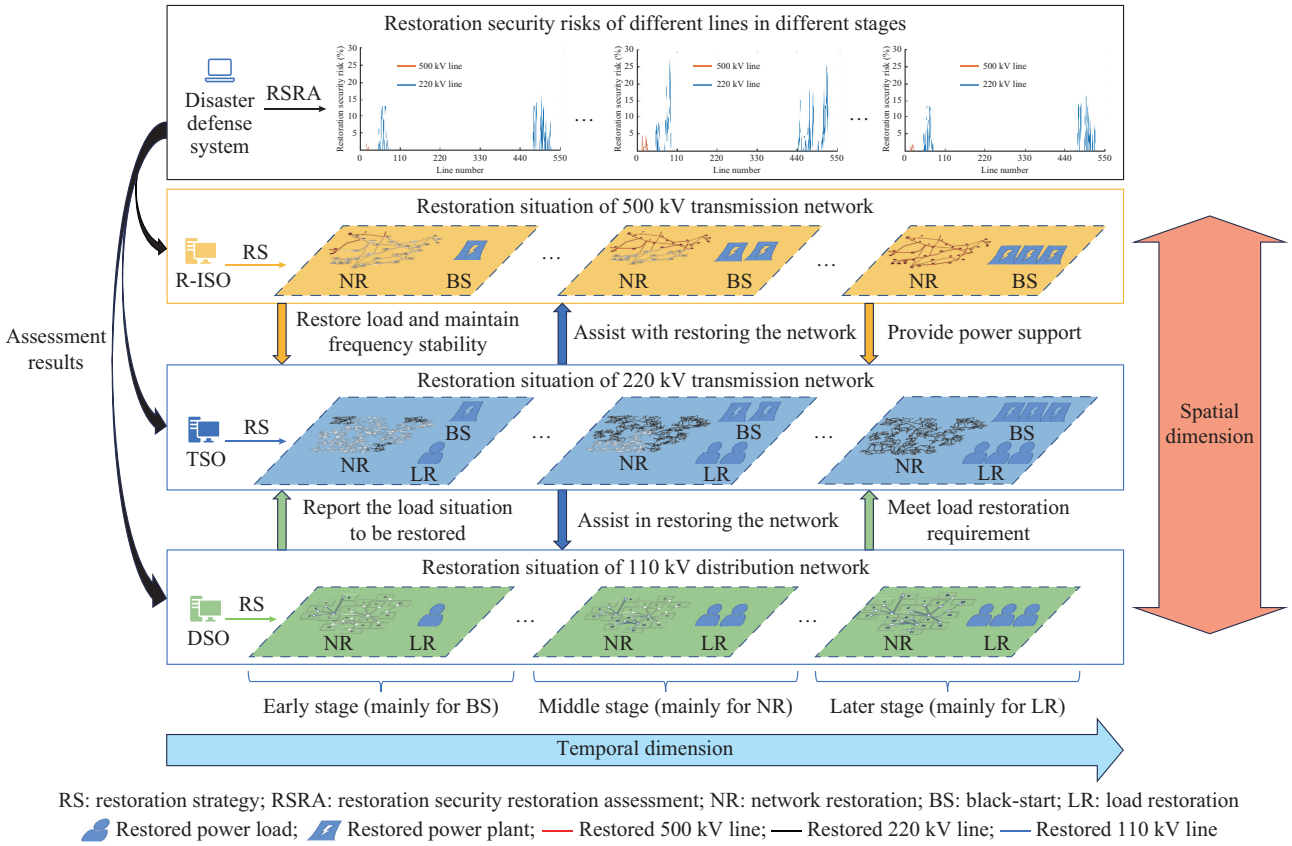

RS: restoration strategy; RSRA: restoration security restoration assessment; NR: network restoration; BS: black-start; LR: load restoration

Restored power load; Restored power plant; Restored 500 kV line; Restored 220 kV line; Restored 110 kV line

Fig. 1. Spatio-temporal coordinated restoration framework for MVLPSs considering restoration security risk assessment.

From a temporal coordination perspective, this paper explores full-stage restoration strategies, covering the entire process from blackout to complete load restoration. In the full-stage restoration process of MVLPSs, the restoration objectives in the early, middle, and later stages are not entirely identical but interconnected. For example, in the 220 kV transmission network managed by TSO, the early stage of restoration focuses on the black start of generators. Additionally, it includes restoring the network path from black-start generators to non-black-start generators while partially restoring loads to maintain frequency stability. In the middle stage of restoration of the 220 kV transmission network, most of the generators and a small portion of critical loads have been restored, requiring further expansion of network and load restoration coverage. In the later stage of restoration of the 220 kV transmission network, when the network and generators are essentially restored, the objective is to restore all loads as quickly as possible, achieving comprehensive restoration of the 220 kV transmission network.

The restoration of the 500 kV transmission network under the jurisdiction of R-ISO and the 110 kV distribution network under the jurisdiction of DSO follows a similar temporal coordination strategy as that of the 220 kV transmission network under the jurisdiction of TSO. The difference lies in the fact that the 500 kV transmission network typically does not directly connect to loads, so the load restoration is not considered by R-ISO. Similarly, 110 kV distribution network usually does not connect to large non-black-start generators, so the black start of generators is not considered by DSO.

From a spatial coordination perspective, R-ISO, TSO, and DSO formulate the full-stage restoration strategies for the 500 kV transmission network, 220 kV transmission network, and 110 kV distribution network, respectively. Due to the existence of coupling buses among MVLPSs, they can realize spatial coordination in the restoration process. Specifically, in the early stage of restoration, DSO needs to report the status of loads to be restored to TSO, enabling TSO to develop corresponding restoration strategies more effectively; R-ISO

needs to restore a portion of TSO's load to maintain system frequency stability. In the middle stage of restoration, TSO supports R-ISO by helping restore non-black-start generators from the bottom up. Simultaneously, it aids DSO in restoring the 110 kV distribution network from the top down, enabling faster load restoration. In the later stage of restoration, R-ISO can provide power support to TSO from top to bottom, while DSO needs to meet the load restoration requirements issued by TSO as much as possible.

In terms of restoration security risks, the disaster defense system assesses the restoration security risks of the 500 kV transmission network, 220 kV transmission network, and 110 kV distribution network at each time step, which is based on the spatio-temporal restoration security risk assessment approach for MVLPSs proposed in Section II-A. Then, the assessment results are communicated from the disaster defense system to R-ISO, TSO, and DSO to provide a reference for the formulation of their spatio-temporal coordinated restoration strategies.

The proposed spatio-temporal coordinated restoration framework for MVLPSs facilitates bottom-up restoration from the TSO to the R-ISO, as well as top-down restoration from the TSO to the DSO. Compared with the traditional two-level restoration framework, this framework better aligns with the hierarchical structure of practical power systems, ensuring that each system operator (R-ISO, TSO, and DSO) can formulate restoration strategies tailored to their respective responsibilities. It also enables power support from the R-ISO to the TSO and facilitates the match of load restoration requirements from the DSO to the TSO. Within this framework, it is necessary to study the optimal spatio-temporal coordinated restoration strategies for MVLPSs during the full-stage restoration process to maximize the net restoration benefits of MVLPSs. The specific restoration optimization model will be presented in Section III.

III. Restoration Security Risk Assessment Based Triple-level Optimization Model for Coordinated Restoration of MVLPSs

In this section, a restoration security risk assessment based triple-level optimization model is proposed for the spatio-temporal coordinated restoration of MVLPSs. Specifically, the restoration benefits of generators, networks, and loads, as well as the control costs associated with restoration security risks, are quantified as economic benefits within the full-stage restoration process of MVLPSs. The impacts of uncertainty in typhoon wind speed and load forecasts are handled using CVaR, and evaluation indicators for the net restoration benefits of MVLPSs are constructed. Then, three submodels are established, whose objective functions are maximizing the net restoration benefits of R-ISO, TSO, and DSO, respectively. Finally, a spatio-temporal coordinated restoration framework based solving process is proposed to solve the proposed triple-level optimization model.

A. Evaluation Indicators for Net Restoration Benefits of MVLPSs

The 500 kV transmission network under the jurisdiction of R-ISO usually does not directly connect to loads but has non-black-start generators of large installed capacity. Hence, the net restoration benefit of R-ISO, i.e., $f^{\text{R-ISO}}$, is related to the power generation restoration benefit $f_{\text{G},t}^{\text{R-ISO}}$, network restoration benefit $f_{\text{N},t}^{\text{R-ISO}}$, restoration security risk control cost $f_{\text{RSR},t}^{\text{R-ISO}}$, and CVaR $M_{\text{CVaR}}^{\text{R-ISO}}$, which is represented by (8). The expression for $f_{\text{RSR},t}^{\text{R-ISO}}$ is similar to (7); the expressions for $f_{\text{G},t}^{\text{R-ISO}}$ and $f_{\text{N},t}^{\text{R-ISO}}$ are given by (9) and (10), respectively; and the expression for $M_{\text{CVaR}}^{\text{R-ISO}}$ is represented by (11) [23].

$$f^{\text{R-ISO}}=\gamma^{\text{R-ISO}}\sum_{t=1}^{T}(f_{\text{G},t}^{\text{R-ISO}}+f_{\text{N},t}^{\text{R-ISO}}-f_{\text{RSR},t}^{\text{R-ISO}})+(1-\gamma^{\text{R-ISO}})M_{\text{CVaR}}^{\text{R-ISO}} \tag{8}$$

$$f_{\text{G},t}^{\text{R-ISO}}=\sum_{n=1}^{N_{\text{bus}}^{\text{R-ISO}}}a_{\text{G,I},n}^{\text{R-ISO}}\int_0^T P_{\text{G},n,t}^{\text{R-ISO,rl}}\text{d}t \tag{9}$$

$$f_{\text{N},t}^{\text{R-ISO}}=a_{\text{bus,I}}^{\text{R-ISO}}\sum_{n=1}^{N_{\text{bus}}^{\text{R-ISO}}}(I_{\text{bus},n,\text{con}}^{\text{R-ISO}}+I_{\text{bus},n,\text{dis}}^{\text{R-ISO}})B_{\text{bus},n,t}^{\text{R-ISO}}+a_{\text{line,I}}^{\text{R-ISO}}\sum_{l=1}^{N_{\text{line}}^{\text{R-ISO}}}I_{\text{line},l,\text{tra}}^{\text{R-ISO}}B_{\text{line},l,t}^{\text{R-ISO}} \tag{10}$$

$$M_{\text{CVaR}}^{\text{R-ISO}}=M_{\text{VaR}}^{\text{R-ISO}}-\frac{\sum_{s=1}^{N_{\text{sce}}}\rho_s\left[M_{\text{VaR}}^{\text{R-ISO}}-\left(\sum_{t=1}^{T}f_{\text{net},t}^{\text{R-ISO}}-f_{\text{loss},s}^{\text{R-ISO}}\right),0\right]^+}{1-\beta_{\text{CVaR}}} \tag{11}$$

where $\gamma^{\text{R-ISO}}$ is the scale coefficient of the CVaR under the jurisdiction of R-ISO; T is the total number of restoration time steps; $a_{\text{G,I},n}^{\text{R-ISO}}$ is the unit net restoration benefit of power generation at bus n under the jurisdiction of R-ISO; $P_{\text{G},n,t}^{\text{R-ISO,rl}}$ is the restored power generation of the generator at bus n under the jurisdiction of R-ISO; $a_{\text{bus,I}}^{\text{R-ISO}}$ and $a_{\text{line,I}}^{\text{R-ISO}}$ are the unit net restoration benefits for buses and lines under the jurisdiction of R-ISO, respectively; $N_{\text{bus}}^{\text{R-ISO}}$ and $N_{\text{line}}^{\text{R-ISO}}$ are the numbers of buses and lines under the jurisdiction of R-ISO, respectively; $B_{\text{bus},n,t}^{\text{R-ISO}}$ and $B_{\text{line},l,t}^{\text{R-ISO}}$ are the restoration state variables for bus n and line l under the jurisdiction of R-ISO, respectively, where a value of 1 indicates restoration and 0 indicates non-restoration; $I_{\text{bus},n,\text{con}}^{\text{R-ISO}}$ and $I_{\text{bus},n,\text{dis}}^{\text{R-ISO}}$ are the connectivity and shortest distance indexes of bus n, respectively [14]; $I_{\text{line},l,\text{tra}}^{\text{R-ISO}}$ is the power transmission capacity index of line l; $M_{\text{VaR}}^{\text{R-ISO}}$ is the value at risk of R-ISO; N_{sce} is the number of typical uncertainty scenarios; ρ_s is the probability of occurrence of scenario s; $f_{\text{net},t}^{\text{R-ISO}}=f_{\text{G},t}^{\text{R-ISO}}+f_{\text{N},t}^{\text{R-ISO}}-f_{\text{RSR},t}^{\text{R-ISO}}$ is the net restoration benefit of R-ISO without considering CvaR; $f_{\text{loss},s}^{\text{R-ISO}}$ is the loss cost incurred due to uncertainty in typhoon wind speed and load forecasts; and β_{CVaR} is the confidence level of CVaR.

The restoration process of 220 kV transmission network under the jurisdiction of TSO includes power generation restoration, network restoration, and load restoration. Hence, the net restoration benefit of TSO f^{TSO} is related to the power generation restoration benefit $f_{\text{G},t}^{\text{TSO}}$, load restoration benefit $f_{\text{L},t}^{\text{TSO}}$, network restoration benefit $f_{\text{N},t}^{\text{TSO}}$, restoration security risk control cost $f_{\text{RSR},t}^{\text{TSO}}$, and CVaR $M_{\text{CVaR}}^{\text{TSO}}$, which is represented by (12). The 110 kV transmission network under the jurisdiction of DSO usually does not have non-black-start genera-

tors of large installed capacity, so the net restoration benefit of DSO f^{DSO} is related to the load restoration benefit $f_{\mathrm{L},t}^{\mathrm{DSO}}$, network restoration benefit $f_{\mathrm{N},t}^{\mathrm{DSO}}$, restoration security risk control cost $f_{\mathrm{RSR},t}^{\mathrm{DSO}}$, and CVaR $M_{\mathrm{CVaR}}^{\mathrm{DSO}}$, which is represented by (13). Note that the expression of $f_{\mathrm{L},t}^{\mathrm{TSO}}$ is represented by (14); the DSO needs to meet the load restoration requirements set by the TSO, so f^{DSO} includes the deviation penalty cost for load restoration, which is represented by (15). Additionally, the expressions for $f_{\mathrm{G},t}^{\mathrm{TSO}}$, $f_{\mathrm{N},t}^{\mathrm{TSO}}$, and $f_{\mathrm{N},t}^{\mathrm{DSO}}$ are similar to (9) and (10), which will not be repeated here.

$$f^{\mathrm{TSO}}=\gamma^{\mathrm{TSO}}\sum_{t=1}^{T}(f_{\mathrm{G},t}^{\mathrm{TSO}}+f_{\mathrm{L},t}^{\mathrm{TSO}}+f_{\mathrm{N},t}^{\mathrm{TSO}}-f_{\mathrm{RSR},t}^{\mathrm{TSO}})+(1-\gamma^{\mathrm{TSO}})M_{\mathrm{CVaR}}^{\mathrm{TSO}} \quad (12)$$

$$f^{\mathrm{DSO}}=\gamma^{\mathrm{DSO}}\sum_{t=1}^{T}(f_{\mathrm{L},t}^{\mathrm{DSO}}+f_{\mathrm{N},t}^{\mathrm{DSO}}-f_{\mathrm{RSR},t}^{\mathrm{DSO}})+(1-\gamma^{\mathrm{DSO}})M_{\mathrm{CVaR}}^{\mathrm{DSO}} \quad (13)$$

$$f_{\mathrm{L},t}^{\mathrm{TSO}}=\sum_{n=1}^{N_{\mathrm{bus}}^{\mathrm{TSO}}}a_{\mathrm{L,I},n}^{\mathrm{TSO}}P_{\mathrm{L},n,t}^{\mathrm{TSO}}\Delta t \quad (14)$$

$$f_{\mathrm{L},t}^{\mathrm{DSO}}=\left(\sum_{n=1}^{N_{\mathrm{bus}}^{\mathrm{DSO}}}a_{\mathrm{L,I},n}^{\mathrm{DSO}}P_{\mathrm{L},n,t}^{\mathrm{DSO}}-a_{\mathrm{L,I,pun}}^{\mathrm{DSO}}\left|P_{\mathrm{L},t}^{\mathrm{TSO}}-\sum_{n=1}^{N_{\mathrm{bus}}^{\mathrm{DSO}}}P_{\mathrm{L},n,t}^{\mathrm{DSO}}\right|\right)\Delta t \quad (15)$$

where γ^{TSO} and γ^{DSO} are the scale coefficients of the CVaR under the jurisdiction of TSO and DSO, respectively; $M_{\mathrm{CVaR}}^{\mathrm{TSO}}$ and $M_{\mathrm{CVaR}}^{\mathrm{DSO}}$ are the values at risk of TSO and DSO, respectively; $N_{\mathrm{bus}}^{\mathrm{TSO}}$ and $N_{\mathrm{bus}}^{\mathrm{DSO}}$ are the numbers of buses under the jurisdiction of TSO and DSO, respectively; $a_{\mathrm{L,I},n}^{\mathrm{TSO}}$ is the unit net restoration benefit of load at bus n under the jurisdiction of TSO; $P_{\mathrm{L},n,t}^{\mathrm{DSO}}$ and $P_{\mathrm{L},n,t}^{\mathrm{TSO}}$ are the restored load power at bus n under the jurisdiction of DSO and TSO, respectively; Δt is the interval between adjacent time steps; $a_{\mathrm{L,I,pun}}^{\mathrm{DSO}}$ is the unit penalty cost for the difference between the restored load power of DSO and the expected restored load power set by the TSO; and $P_{\mathrm{L},t}^{\mathrm{TSO}}$ is the expected restored load power set by the TSO.

B. Upper-level Restoration Optimization Submodel for R-ISO

The objective function of the upper-level submodel is to maximize the net restoration benefit of R-ISO, which is represented by (16). The constraints of the upper-level submodel are represented by (17)-(26). Among them, the black-start constraints are expressed as (17)-(22); the network restoration constraints are presented in (23)-(25); the power balance constraint is shown in (26); and the transmission network power flow and security constraints refer to [19]. Note that during typhoon disasters, photovoltaic power plants do not generate power due to cloudy and rainy weather, while the wind speed during typhoon disasters typically exceeds the cut-out wind speed for wind turbines, resulting in no power generation from wind power plants.

$$\max f^{\mathrm{R\text{-}ISO}} \quad (16)$$

$$P_{\mathrm{G},n,t}^{\mathrm{R\text{-}ISO,rl}}=\begin{cases}0 & t<T_{\mathrm{G},n}^{\mathrm{R\text{-}ISO,st}}\\ (t-T_{\mathrm{G},n}^{\mathrm{R\text{-}ISO,st}})R_{\mathrm{G},n}^{\mathrm{R\text{-}ISO,rp}}-P_{\mathrm{G},n}^{\mathrm{R\text{-}ISO,st}} & T_{\mathrm{G},n}^{\mathrm{R\text{-}ISO,st}}\le t<T_{\mathrm{G},n}^{\mathrm{R\text{-}ISO,st}}+T_{\mathrm{G},n}^{\mathrm{R\text{-}ISO,rp}}\\ P_{\mathrm{G},n}^{\mathrm{R\text{-}ISO,max}}-P_{\mathrm{G},n}^{\mathrm{R\text{-}ISO,st}} & t\ge T_{\mathrm{G},n}^{\mathrm{R\text{-}ISO,st}}+T_{\mathrm{G},n}^{\mathrm{R\text{-}ISO,rp}}\end{cases} \quad (17)$$

$$T_{\mathrm{G},n}^{\mathrm{R\text{-}ISO,st,min}}\le T_{\mathrm{G},n}^{\mathrm{R\text{-}SO,st}}\le T_{\mathrm{G},n}^{\mathrm{R\text{-}ISO,st,max}} \quad (18)$$

$$\sum_{t=1}^{T}(1-B_{\mathrm{G},n,t}^{\mathrm{R\text{-}ISO}})\le T_{\mathrm{G},n}^{\mathrm{R\text{-}ISO,st}} \quad (19)$$

$$T_{\mathrm{BG},n}^{\mathrm{R\text{-}ISO,st}}=0 \quad (20)$$

$$B_{\mathrm{BG},n,t}^{\mathrm{R\text{-}ISO}}=1 \quad t\ge 1 \quad (21)$$

$$\sum_{t=1}^{T}(1-B_{\mathrm{line},l,t}^{\mathrm{R\text{-}ISO}})\ge T_{\mathrm{G},n}^{\mathrm{R\text{-}ISO,st}} \quad \forall l\in\Omega_{\mathrm{line,bus},n}^{\mathrm{R\text{-}ISO}} \quad (22)$$

$$\begin{cases}B_{\mathrm{bus},n,t}^{\mathrm{R\text{-}ISO}}\ge B_{\mathrm{bus},n,t-1}^{\mathrm{R\text{-}ISO}}\\ B_{\mathrm{line},l,t}^{\mathrm{R\text{-}ISO}}\ge B_{\mathrm{line},l,t-1}^{\mathrm{R\text{-}ISO}}\\ B_{\mathrm{line},p,t}^{\mathrm{R\text{-}ISO}}\le \sum\limits_{\forall q\in\Omega_{\mathrm{line,line},p}^{\mathrm{R\text{-}ISO}}}B_{\mathrm{line},q,t-1}^{\mathrm{R\text{-}ISO}}\end{cases} \quad (23)$$

$$B_{\mathrm{bus},n,t}^{\mathrm{R\text{-}ISO}}\ge B_{\mathrm{line},l,t}^{\mathrm{R\text{-}ISO}} \quad \forall l\in\Omega_{\mathrm{line,bus},n}^{\mathrm{R\text{-}ISO}} \quad (24)$$

$$B_{\mathrm{bus},n,t}^{\mathrm{R\text{-}ISO}}\le \sum_{l\in\Omega_{\mathrm{line,bus},n}^{\mathrm{R\text{-}ISO}}}B_{\mathrm{line},l,t}^{\mathrm{R\text{-}ISO}} \quad (25)$$

$$P_{\mathrm{BG},n,t}^{\mathrm{R\text{-}ISO}}+P_{\mathrm{G},n,t}^{\mathrm{R\text{-}ISO,rl}}+P_{\mathrm{O\text{-}TSO},n,t}^{\mathrm{R\text{-}ISO}}=P_{\mathrm{TSO},n,t}^{\mathrm{R\text{-}ISO}} \quad (26)$$

where $P_{\mathrm{G},n,t}^{\mathrm{R\text{-}ISO,rl}}$ is the power of non-black-start generator in 500 kV transmission network; $T_{\mathrm{G},n}^{\mathrm{R\text{-}ISO,st}}$ is the start time of the non-black-start generator; $T_{\mathrm{G},n}^{\mathrm{R\text{-}ISO,rp}}$ is the time required for the non-black-start generator to reach its rated power after starting, $T_{\mathrm{G},n}^{\mathrm{R\text{-}ISO,rp}}=(P_{\mathrm{G},n}^{\mathrm{R\text{-}ISO,max}}-P_{\mathrm{G},n}^{\mathrm{R\text{-}ISO,st}})/R_{\mathrm{G},n}^{\mathrm{R\text{-}ISO,rp}}$; $P_{\mathrm{G},n}^{\mathrm{R\text{-}ISO,max}}$ is the rated power of the non-black-start generator; $P_{\mathrm{G},n}^{\mathrm{R\text{-}ISO,st}}$ is the auxiliary power required for the start-up of the non-black-start generator; $R_{\mathrm{G},n}^{\mathrm{R\text{-}ISO,rp}}$ is the maximum ramp rate of the non-black-start generator; $T_{\mathrm{G},n}^{\mathrm{R\text{-}ISO,st,max}}$ and $T_{\mathrm{G},n}^{\mathrm{R\text{-}ISO,st,min}}$ are the upper and lower bounds on the start-up time of the non-black-start generator, respectively; $B_{\mathrm{G},n,t}^{\mathrm{R\text{-}ISO}}$ and $B_{\mathrm{BG},n,t}^{\mathrm{R\text{-}ISO}}$ are the binary variables indicating the start-up statuses of the non-black-start and black-start generators, respectively, with a value of 1 indicating that the generator has been started; $T_{\mathrm{BG},n}^{\mathrm{R\text{-}ISO,st}}$ is the start time of the black-start generator; $B_{\mathrm{line},l,t}^{\mathrm{R\text{-}ISO}}$ is the restoration status of line l, with a value of 1 indicating that the line is restored; $\Omega_{\mathrm{line,bus},n}^{\mathrm{R\text{-}ISO}}$ is the set of lines connected to bus n; $B_{\mathrm{line},p,t}^{\mathrm{R\text{-}ISO}}$ and $B_{\mathrm{line},q,t-1}^{\mathrm{R\text{-}ISO}}$ are the restoration statuses of line p at time step t and line q at time step $t-1$, respectively; $\Omega_{\mathrm{line,line},p}^{\mathrm{R\text{-}ISO}}$ is the set of lines connected to line p; $P_{\mathrm{BG},n,t}^{\mathrm{R\text{-}ISO}}$ is the output power of black-start generator at bus n; $P_{\mathrm{O\text{-}TSO},n,t}^{\mathrm{R\text{-}ISO}}$ is the power supplied to the R-ISO by other TSOs; and $P_{\mathrm{TSO},n,t}^{\mathrm{R\text{-}ISO}}$ is the power exchange between the R-ISO and TSO, where a positive value indicates that the R-ISO is supplying power to the TSO, while a negative value indicates that the R-ISO is requesting power support from the TSO.

C. Middle-level Restoration Optimization Submodel for TSO

The objective function of the middle-level submodel f^{TSO} is to maximize the net restoration benefit of TSO, which is represented by (27). The constraints of the middle-level submodel have additional load restoration constraints compared with those of the upper-level submodel. More specifically, the load restoration constraints are represented by (28)-(30); the power balance constraint is shown in (31); the black-start constraints are similar to (17)-(22); the network restoration constraints are similar to (23)-(25); the transmission network power flow and security constraints refer to [19] and [25]; and the operational constraints of energy storage devic-

es can be found in [26].

$$\max f^{\mathrm{TSO}} \tag{27}$$

$$B^{\mathrm{TSO}}_{\mathrm{bus,L},n,t} \le B^{\mathrm{TSO}}_{\mathrm{bus},n,t} \tag{28}$$

$$P^{\mathrm{TSO}}_{\mathrm{L},n,t} = B^{\mathrm{TSO}}_{\mathrm{bus,L},n,t} P^{\max}_{\mathrm{L},n} \tag{29}$$

$$0 \le B^{\mathrm{TSO}}_{\mathrm{bus,L},n,t-1} \le B^{\mathrm{TSO}}_{\mathrm{bus,L},n,t} \quad \forall n \in \Omega^{\mathrm{TSO}}_{\mathrm{bus,IFL}} \tag{30}$$

$$P^{\mathrm{TSO,rl}}_{\mathrm{G},n,t} + P^{\mathrm{TSO}}_{\mathrm{BG},n,t} + P^{\mathrm{TSO,dis}}_{\mathrm{ES},n,t} = P^{\mathrm{TSO}}_{\mathrm{L},n,t} + P^{\mathrm{TSO}}_{\mathrm{R\text{-}ISO},n,t} + P^{\mathrm{TSO,cha}}_{\mathrm{ES},n,t} \tag{31}$$

where $B^{\mathrm{TSO}}_{\mathrm{bus,L},n,t}$ is the binary variable representing the load restoration status at bus n, with a value of 1 indicating the start of load restoration; $P^{\mathrm{TSO}}_{\mathrm{L},n,t}$ and $P^{\max}_{\mathrm{L},n}$ are the restored load power and the maximum load power to be restored at bus n, respectively; $\Omega^{\mathrm{TSO}}_{\mathrm{bus,IFL}}$ is the set of buses where inflexible loads are located; $P^{\mathrm{TSO,rl}}_{\mathrm{G},n,t}$ is the power of non-black-start generator in 220 kV transmission network; $P^{\mathrm{TSO}}_{\mathrm{BG},n,t}$ is the output power of black-start generator at bus n; $P^{\mathrm{TSO,dis}}_{\mathrm{ES},n,t}$ and $P^{\mathrm{TSO,cha}}_{\mathrm{ES},n,t}$ are the charging and discharging power of energy storage devices at bus n, respectively; and $P^{\mathrm{TSO}}_{\mathrm{R\text{-}ISO},n,t}$ is the interaction power between the TSO and R-ISO, where a positive value indicates that the TSO provides power to the R-ISO, and a negative value indicates that the TSO requests power support from the R-ISO.

D. Lower-level Restoration Optimization Submodel for DSO

The objective function of the lower-level submodel is to maximize the net restoration benefit of DSO, which is represented by (32). The constraints of the lower-level submodel do not have black-start constraints compared with those of the middle-level submodel. Specifically, the network restoration constraints are similar to (23)-(25); the load restoration constraints are similar to (28)-(30); the power balance constraint is shown in (33); and the power flow and security constraints of the distribution network refer to [14].

$$\max f^{\mathrm{DSO}} \tag{32}$$

$$P^{\mathrm{DSO,dis}}_{\mathrm{ES},n,t} = P^{\mathrm{DSO}}_{\mathrm{L},n,t} + P^{\mathrm{DSO}}_{\mathrm{TSO},n,t} + P^{\mathrm{DSO,cha}}_{\mathrm{ES},n,t} \tag{33}$$

where $P^{\mathrm{DSO,dis}}_{\mathrm{ES},n,t}$ and $P^{\mathrm{DSO,cha}}_{\mathrm{ES},n,t}$ are the charging and discharging power of energy storage devices at bus n, respectively; and $P^{\mathrm{DSO}}_{\mathrm{TSO},n,t}$ is the interaction power between the DSO and TSO, where a positive value indicates that the DSO provides power to the TSO, and a negative value indicates that the DSO requests power support from the TSO.

E. Solving Process for Triple-level Optimization Model

In this subsection, a solving process for the triple-level optimization model is proposed according to the spatio-temporal coordinated restoration framework proposed in Section III, whose procedure is shown as follows.

Step 1: input network data of MVLPSs, predictive information of typhoon wind speed and path, and evaluation indicators of the restoration security risk of each line at MVLPSs.

Step 2: the TSO collects the predicted matrix of load demand to be restored at each time step from $N^{\mathrm{TSO}}_{\mathrm{DSO,bus}}$ DSOs, denoted as $\boldsymbol{P}^{\max}_{\mathrm{L},d} = [P^{\max}_{\mathrm{L},d,1}, ..., P^{\max}_{\mathrm{L},d,2}, ..., P^{\max}_{\mathrm{L},d,T}]$ $(d = 1, 2, \ldots, N^{\mathrm{TSO}}_{\mathrm{DSO,bus}})$. Set $d = 1$.

Step 3: solve the initial middle-level submodel. By solving the initial middle-level submodel established in Section IV-B, the TSO can obtain the initial restoration strategies for the 220 kV transmission network without considering power interactions with the R-ISO.

Step 4: transmit restoration information from the TSO to the R-ISO and DSOs. The TSO transmits the matrix of minimum restoration steps for $N^{\mathrm{TSO}}_{\mathrm{R\text{-}ISO,bus}}$ R-ISO and TSO coupling buses, denoted as $\boldsymbol{t}^{\mathrm{TSO}}_{\mathrm{R\text{-}ISO,bus}} = [t^{\mathrm{TSO}}_{\mathrm{R\text{-}ISO,bus},1}, t^{\mathrm{TSO}}_{\mathrm{R\text{-}ISO,bus},2}, ..., t^{\mathrm{TSO}}_{\mathrm{R\text{-}ISO,bus},N^{\mathrm{TSO}}_{\mathrm{R\text{-}ISO,bus}}}]$, to the R-ISO. Simultaneously, the TSO provides all $N^{\mathrm{TSO}}_{\mathrm{DSO,bus}}$ TSO and DSO coupling buses with the matrix of minimum restoration time steps, denoted as $\boldsymbol{t}^{\mathrm{TSO}}_{\mathrm{DSO,bus}} = [t^{\mathrm{TSO}}_{\mathrm{DSO,bus},1}, t^{\mathrm{TSO}}_{\mathrm{DSO,bus},2}, ..., t^{\mathrm{TSO}}_{\mathrm{DSO,bus},N^{\mathrm{TSO}}_{\mathrm{DSO,bus}}}]$, and the matrix of expected load power restoration at each time step for each DSO, denoted as $\boldsymbol{P}^{\mathrm{TSO}}_{\mathrm{L},d} = [P^{\mathrm{TSO}}_{\mathrm{L},d,1}, P^{\mathrm{TSO}}_{\mathrm{L},d,2}, ..., P^{\mathrm{TSO}}_{\mathrm{L},d,T}]$ $(d = 1, 2, ..., N^{\mathrm{TSO}}_{\mathrm{DSO,bus}})$.

Step 5: solve the upper-level submodel. The upper-level submodel is established in Section IV-C. Note that the upper-level submodel incorporates an additional constraint for the minimum restoration of the R-ISO and TSO coupling buses according to its received $\boldsymbol{t}^{\mathrm{TSO}}_{\mathrm{RTO,bus}}$, as shown in (34). This constraint ensures that if the R-ISO and TSO coupling bus n cannot be restored before the minimum restoration time step $t^{\mathrm{TSO}}_{\mathrm{R\text{-}ISO,bus},n}$, it can act as a black-start source bus to assist the R-ISO from bottom to top in restoring the network structure after $t^{\mathrm{TSO}}_{\mathrm{R\text{-}ISO,bus},n}$. By solving the upper-level submodel, the black-start and network reconfiguration strategies for the 500 kV transmission network can be obtained.

$$B^{\mathrm{R\text{-}ISO}}_{\mathrm{bus},n,t} = \begin{cases} 0 \text{ or } 1 & t < t^{\mathrm{TSO}}_{\mathrm{R-ISO,bus},n} \\ 1 & t \ge t^{\mathrm{TSO}}_{\mathrm{R-ISO,bus},n} \end{cases} \tag{34}$$

where $B^{\mathrm{R\text{-}ISO}}_{\mathrm{bus},n,t}$ is the restoration state variable for bus n.

Step 6: provide the restoration information feedback from the R-ISO to the TSO. The R-ISO provides feedback to the TSO by transmitting the matrix of final restoration time steps for $N^{\mathrm{TSO}}_{\mathrm{R\text{-}ISO,bus}}$ R-ISO and TSO coupling buses, denoted as $\boldsymbol{t}^{\mathrm{R\text{-}ISO}}_{\mathrm{TSO,bus}} = [t^{\mathrm{R\text{-}ISO}}_{\mathrm{TSO,bus},1}, t^{\mathrm{R\text{-}ISO}}_{\mathrm{TSO,bus},2}, ..., t^{\mathrm{R\text{-}ISO}}_{\mathrm{TSO,bus},N^{\mathrm{R\text{-}ISO}}_{\mathrm{TSO,bus}}}]$, as well as the matrix of available unit power at each time step, denoted as $\boldsymbol{P}^{\mathrm{R\text{-}ISO}}_{\mathrm{G}} = [P^{\mathrm{R\text{-}ISO}}_{\mathrm{G},1}, P^{\mathrm{R\text{-}ISO}}_{\mathrm{G},2}, ..., P^{\mathrm{R\text{-}ISO}}_{\mathrm{G},T}]$. This feedback enables the TSO to further refine its load power restoration strategy based on the updated information provided by the R-ISO.

Step 7: solve the d^{th} lower-level submodel. The d^{th} lower-level submodel is established in Section IV-D. Note that the lower-level submodel incorporates an additional constraint for the minimum restoration of the TSO and DSO coupling buses according to its received $t^{\mathrm{TSO}}_{\mathrm{DSO,bus},d}$, as shown in (35). This constraint ensures that if the TSO and DSO coupling bus d cannot be restored before the minimum restoration time step $t^{\mathrm{TSO}}_{\mathrm{DSO,bus},d}$, it can act as a black-start source bus to assist the d^{th} DSO from top to bottom in restoring the network structure after $t^{\mathrm{TSO}}_{\mathrm{DSO,bus},d}$. By solving the d^{th} lower-level submodel, the network reconfiguration and load restoration strategies for the 110 kV distribution network can be obtained.

$$B^{\mathrm{DSO}}_{\mathrm{R\text{-}ISO,bus},d,t} = \begin{cases} 0 \text{ or } 1 & t < t^{\mathrm{TSO}}_{\mathrm{DSO,bus},d} \\ 1 & t \ge t^{\mathrm{TSO}}_{\mathrm{DSO,bus},d} \end{cases} \tag{35}$$

where $B^{\mathrm{DSO}}_{\mathrm{R\text{-}ISO,bus},d,t}$ is the restoration state variable for the TSO and DSO coupling bus d.

Step 8: judge if d is larger than $N^{\mathrm{TSO}}_{\mathrm{DSO,bus}}$. If yes, go to *Step 9*; otherwise, set $d = d + 1$, and return to *Step 7*.

Step 9: provide restoration information feedback from the DSOs to the TSO. $N^{\mathrm{TSO}}_{\mathrm{DSO,bus}}$ DSOs provide feedback to the TSO by transmitting the matrix $\boldsymbol{P}^{\mathrm{DSO}}_{\mathrm{L},d}$ = [$P^{\mathrm{DSO}}_{\mathrm{L},d,1}$, $P^{\mathrm{DSO}}_{\mathrm{L},d,2}$, ..., $P^{\mathrm{DSO}}_{\mathrm{L},d,T}$] ($d$ = 1, 2, ..., $N^{\mathrm{TSO}}_{\mathrm{DSO,bus}}$) containing the actual restored load power at each time step.

Step 10: solve the final middle-level submodel. After receiving the feedback from the R-ISO and DSOs, including matrices $\boldsymbol{t}^{\mathrm{R\text{-}ISO}}_{\mathrm{TSO,bus}}$, $\boldsymbol{P}^{\mathrm{RTO}}_{\mathrm{G}}$, and $\boldsymbol{P}^{\mathrm{DSO}}_{\mathrm{L},d}$, the final middle-level submodel is established by incorporating additional constraints into the initial middle-level submodel. Specifically, it introduces the constraints shown in (36) and (37) to account for the available generation power constraint of the R-ISO and the constraint on the actual restored load power of the DSOs. By solving the final middle-level submodel, the TSO obtains the final restoration strategies for the 220 kV transmission network and provides the power interaction strategy matrix $\boldsymbol{P}^{\mathrm{TSO}}_{\mathrm{R\text{-}ISO}}$=[$P^{\mathrm{TSO}}_{\mathrm{R\text{-}ISO},1}$, $P^{\mathrm{TSO}}_{\mathrm{R\text{-}ISO},2}$, ..., $P^{\mathrm{TSO}}_{\mathrm{R\text{-}ISO},T}$] to the R-ISO for implementation.

$$0 \le P^{\mathrm{TSO}}_{\mathrm{R\text{-}ISO},t} \le P^{\mathrm{TSO}}_{\mathrm{G},t} \tag{36}$$

$$P^{\mathrm{TSO}}_{\mathrm{L},d,t} = P^{\mathrm{DSO}}_{\mathrm{L},d,t} \tag{37}$$

Step 11: output the spatio-temporal coordinated restoration strategies for the 500 kV, 220 kV, and 110 kV distribution networks.

The flowchart of the solving process for the proposed model is shown in Supplementary Material A Fig. SA2. The proposed framework follows a hierarchical coordination structure that aligns with real-world power systems, where restoration decisions for the 500 kV, 220 kV, and 110 kV distribution networks are optimized at the R-ISO, TSO, and DSO levels, respectively. The solving process begins with the TSO optimizing the initial full-stage restoration strategy for the 220 kV distribution network, without considering power interactions with the R-ISO. The results, including generator start-up schedules, network reconfiguration decisions, and expected power exchange with the R-ISO and DSOs, are then transmitted to the respective operators. The R-ISO then solves its optimization model for the 500 kV distribution network, incorporating the expected power exchange constraints from the TSO to determine black-start strategies and network reconfiguration plans, and subsequently provides feedback to the TSO regarding final restoration time steps and available power supply. Meanwhile, DSOs solve their respective models for the 110 kV distribution network, determining load restoration sequences and utilizing the available power supply from the TSO. The DSOs also provide feedback to the TSO regarding the actual restored load power at each time step. With the updated information from both the R-ISO and DSOs, the TSO refines its restoration strategy by solving the final middle-level submodel for the 220 kV distribution network. The final restoration strategies for all voltage levels are then determined and implemented. This structured decision exchange mechanism ensures computational efficiency by reducing unnecessary iterative exchanges and allowing each level to optimize its restoration plan with only a single round of decision exchange, achieving a practical and scalable solution for large-scale power system restoration after major blackouts.

IV. Case Studies

An actual 379-bus MVLPS in China is employed to verify the effectiveness of the proposed method, whose topology is shown in Fig. 2.

Two distribution networks under the jurisdiction of DSOs at buses 79 and 299 are illustrated as examples. When a province-level blackout occurs, it involves power systems across voltage levels of 500 kV (managed by the R-ISO), 220 kV (managed by the TSO), 110 kV and below (managed by the DSO). This MVLPS consists of 16 partitions, including 36 500 kV buses and 343 220 kV buses, with each 220 kV bus connected to a 110 kV distribution network. This MVLPS comprises 6 500 kV power plants and 51 220 kV power plants, among which 8 are black-start power plants (marked with yellow boxes in Fig. 2). The time step is set to be 5 min, which is a widely recognized interval in the existing literature on restoration processes [14]. For detailed information regarding unit installed capacities, line capacities, and other technical specifications, please refer to [27]. The proposed model is implemented on the Yalmip platform in MATLAB 2023a and solved by the Gurobi 11.0 solver.

A. Restoration Security Risks of Various Transmission Lines Under Typhoon Disasters

Wind speeds vary across transmission lines either at different time steps or between different lines at the same time step, resulting in corresponding variations in restoration security risks. To illustrate the spatio-temporal characteristics of these risks, four representative lines, i.e., lines 232-379, 37-38, 15-286, and 10-11, are selected as examples. Their respective typhoon wind speeds and restoration security risks are depicted in Fig. 3. In Fig. 3, the double headed arrows represent the corresponding relationship between typhoon wind speeds and restoration security risks of each transmission line. Specifically, line 232-379 is situated in the landfall region of the typhoon. Around the 11$^{\mathrm{th}}$ time step, it is closest to the typhoon center and experiences a wind speed of 29.1 m/s, exceeding its design limit of 23.5 m/s and resulting in a restoration security risk of 7%. In contrast, line 37-38 is located inland, far from the typhoon path, and encounters a maximum wind speed of only 11.2 m/s, leading to no restoration risk. Line 15-286 lies along the central path of the typhoon, which passes over the line between the 18$^{\mathrm{th}}$ and 33$^{\mathrm{rd}}$ time steps. Due to the intersection with the typhoon wind field, the line is exposed to two peaks in wind speed, with the highest reaching 34.5 m/s. This corresponds to a restoration security risk of 32.1%. Line 10-11, located at the tail end of the typhoon trajectory, experiences a peak wind speed of 32.4 m/s. However, as a 500 kV transmission line has a higher design threshold of 27 m/s, its associated restoration security risk is limited to 4.6%. In summary, the proposed restoration method effectively captures wind speed variations and accurately assesses restoration security risks for transmission lines under extreme weather conditions.

B. Network Restoration Strategies of MVLPSs

The restoration strategy for the 500 kV distribution network of the R-ISO is shown in Fig. 4.

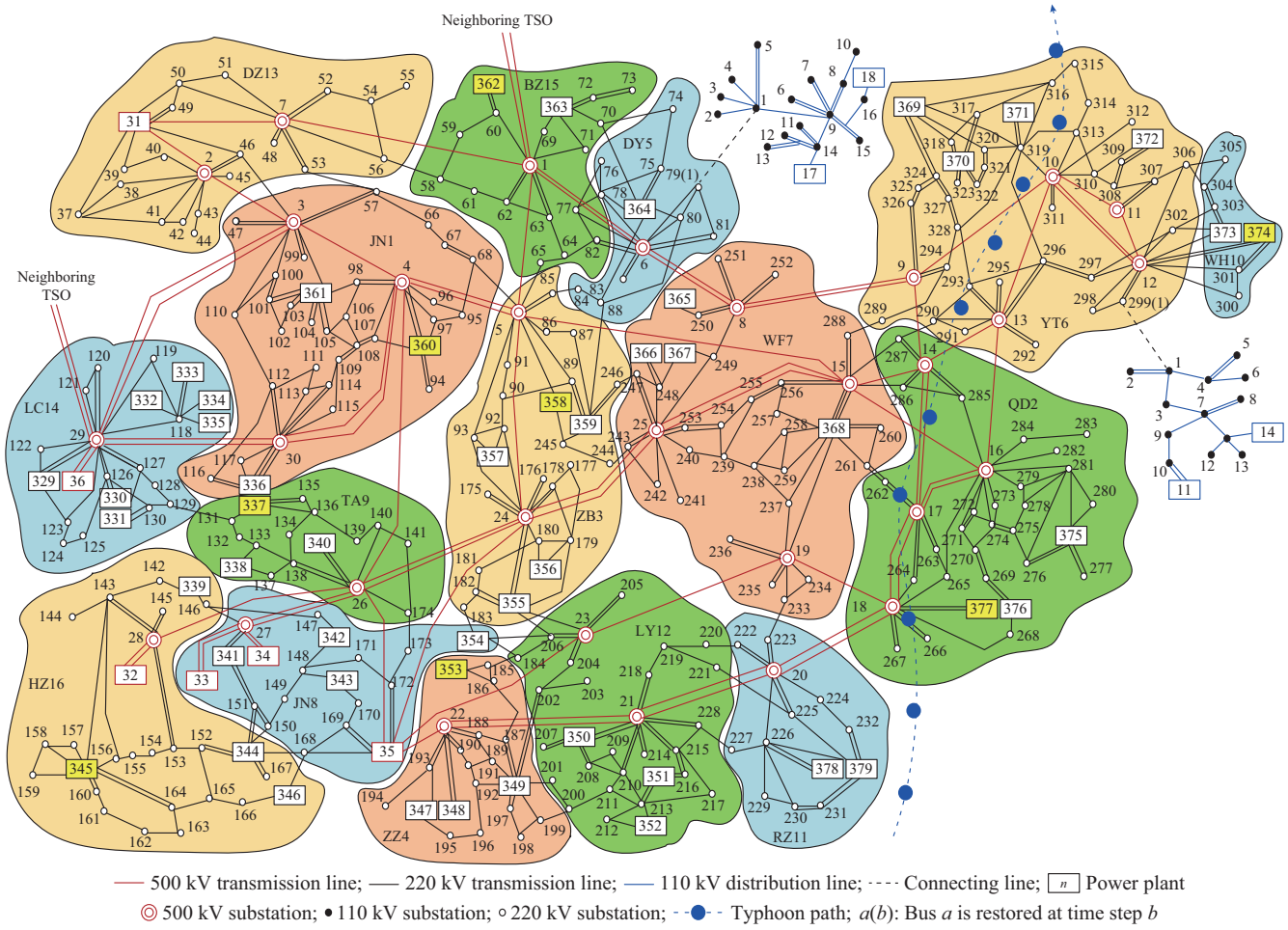

Fig. 2. Topology of an actual 379-bus MVLPS in China.

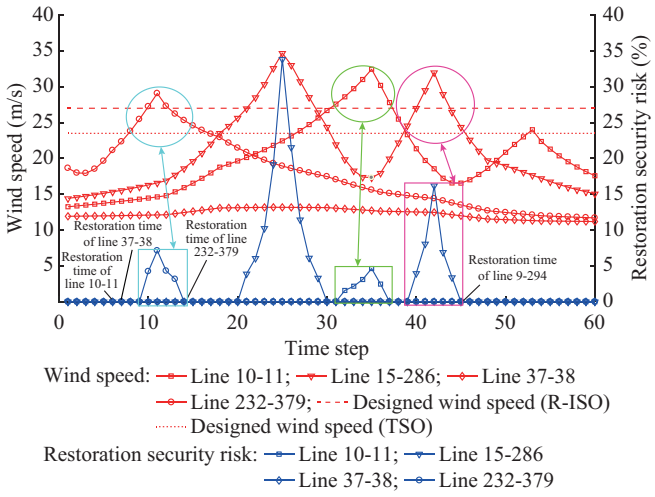

Fig. 3. Typhoon wind speeds and restoration security risks of each transmission line at each time step.

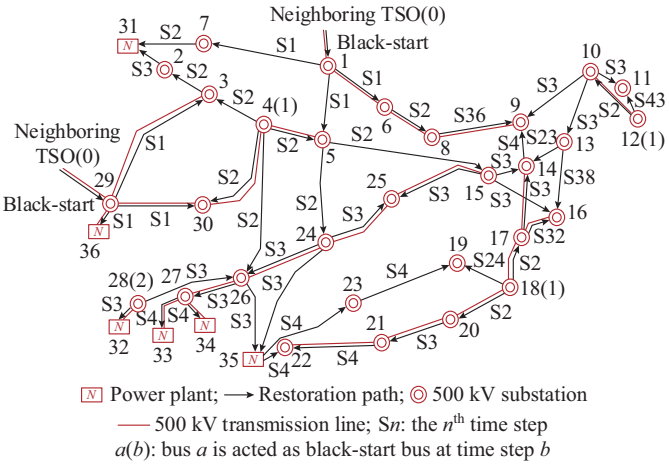

Fig. 4. Restoration strategy for 500 kV distribution network of R-ISO.

It can be observed from Fig. 4 that the neighboring substations connected to the TSO serve as black-start sources following the provincial blackout, enabling the R-ISO to draw power from adjacent TSOs and initiate its black-start operations. Buses 4, 12, and 18 are successfully restored by the TSO at the first time step.

Consequently, these buses also act as black-start buses for the R-ISO, starting from the second time step. Subsequently, the TSO assists the R-ISO in the bottom-up restoration of the network. After four steps, 87.2% of the 500 kV transmission lines are restored. The remaining transmission lines 13-14, 18-19, 16-17, 8-9, 13-16, and 118-12 are restored at the 23rd, 24th, 32nd, 36th, 38th, and 43rd time steps, respectively. This is because these lines are situated in the typhoon path.

Therefore, restoring them before the arrival of typhoon may lead to secondary blackouts due to the high restoration security risks associated with the passage of the typhoon through these lines, thereby resulting in additional control costs. Additionally, since the buses at both ends of these lines have already been restored through other transmission lines, the restoration of these lines is relatively less urgent. Hence, delaying their restoration to time steps with lower restoration security risks can effectively reduce control costs during the restoration process, and enhance the net restoration benefit.

The restoration strategy for the 220 kV distribution network of the TSO is analyzed as follows. Considering that the 220 kV distribution network encompasses 16 cities, the restoration strategies for four representative cities are selected and presented in Supplementary Material A Table SAI. Specifically, RZ11 is a city without a black-start unit and located far away from the typhoon path, YT6 is a city without a black-start unit situated in the typhoon path, JN1 is a city with a black-start unit located far from the typhoon path, and QD2 is a city with a black-start unit situated in the typhoon path. Table SAI shows that RZ11 restores its first bus 223 at the 9th time step with assistance from bus 233 via WF7. Subsequently, RZ11 completes its network restoration by the 13th time step. JN1 has a black-start unit at bus 360 and is situated far from the typhoon path, so it experiences relatively low restoration security risks and successfully restores its network by the 7th time step. YT6 has not a black-start unit, so it relies on the black-start unit at bus 374 of the adjacent city WH10 for network restoration. However, due to its location at the end of the typhoon path, YT6 restores its bus 11 only by the 43rd time step to mitigate additional control costs resulting from restoration security risks. QD2, situated in the middle of the typhoon path, conducts its network restoration through the black-start unit at bus 377. Similarly, bus 14 in QD2 is restored at the 39th time step considering the restoration security risks.

Each 220 kV bus is interconnected with a 110 kV distribution network under the jurisdiction of the DSO. To illustrate their restoration strategies, the 110 kV distribution networks connected to the 220 kV substations at buses 79 and 299 are selected as representative cases for analysis, as shown in Fig. 5.

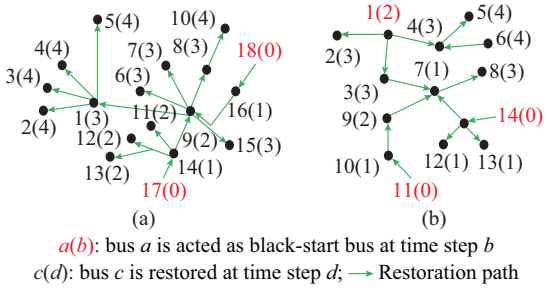

Fig. 5. Restoration strategies for 110 kV distribution networks at buses 79 and 299. (a) 110 kV distribution network at bus 79 (restored by itself). (b) 110 kV distribution network at bus 299 (restored with help of TSO).

For the 110 kV distribution network at bus 79, according to the restoration strategy for the 220 kV distribution network of the TSO, the TSO and DSO coupling bus 1 is scheduled to be restored at the 5th time step. As a result, DSO 79 cannot receive top-down assistance from the TSO before this time step. Therefore, DSO 79 adopts an independent bottom-up restoration strategy by utilizing energy storage devices at buses 17 and 18 as black-start units, completing the restoration of its network within four time steps. Similarly, regarding the 110 kV distribution network at bus 299, as the TSO restores the provincial-local coupling bus 1 at the 2nd time step, DSO 299 can obtain black-start support via bus 1, which is energized by the TSO, and initiate a top-down restoration of its distribution network, thereby completing its network restoration within four time steps.

C. Coordinated Restoration Strategies of R-ISO, TSO, and DSOs

The coordinated restoration strategy between the R-ISO and TSO is analyzed first. Table I presents the minimum restoration time step of the TSO and the actual restoration time step of the R-ISO for 500 kV buses. It can be observed from Table I that 83.3% of the 500 kV buses are restored before the minimum restoration time step of the TSO. This indicates that the R-ISO restores its network by obtaining power from neighboring provinces through the interconnecting buses. Buses 4, 5, 12, 18, 23, and 28 are highlighted in bold in Table I, indicating that they are restored after the minimum restoration time step of the TSO. This restoration strategy demonstrates that after the TSO provides the bus restoration information to the R-ISO, the R-ISO can formulate a restoration strategy that minimizes the overall restoration cost based on the current status of its network. For buses in remote areas that cannot be restored within the required timeframe, the TSO can assist in their restoration after their minimum restoration time steps, thereby achieving bottom-up assistance in the network restoration of the R-ISO.

The coordinated power exchange strategy between the R-ISO and TSO is shown in Fig. 6. In Fig. 6, the red-circle curve represents the power support that the TSO expects to receive from the R-ISO, which is determined by solving the initial middle-level submodel. After receiving the TSO's restoration strategy that minimizes the cost of restoring the coupling buses with the R-ISO, the R-ISO formulates its black-start strategy by the upper-level submodel and provides the upper limit of the power that it can supply to the TSO, which is shown as the blue-diamond curve in Fig. 6. Subsequently, the TSO utilizes this upper limit as a boundary constraint in the final middle-level submodel, and determines the final coordinated power exchange strategy between the R-ISO and TSO, represented by the green-triangle curve in Fig. 6. Consequently, the expected and actual load power restoration of the TSO has a certain deviation, as shown in red and blue curves, respectively. This final strategy accounts for the constraints and requirements of both the R-ISO and TSO, ensuring a coordinated and optimized power exchange between the R-ISO and TSO. Note that the difference between the blue and green curves represents the power deviation between the actual restored load of the DSO and the target load assigned by the TSO.

TABLE I
THE MINIMUM AND ACTUAL RESTORATION TIME STEP OF R-ISO FOR 500 KV BUSES

Bus	The minimum restoration time step	Actual restoration time step	Bus	The minimum restoration time step	Actual restoration time step	Bus	The minimum restoration time step	Actual restoration time step
1	2	1	13	4	3	25	4	3
2	6	2	14	39	3	26	4	2
3	4	1	15	6	2	27	5	3
4	**1**	**1**	16	3	3	**28**	**2**	**2**
5	**1**	**1**	17	3	2	29	5	1
6	5	1	**18**	**1**	**1**	30	5	1
7	5	1	19	7	5	31	6	2
8	6	2	20	10	2	32		3
9	10	3	21	9	3	33		4
10	6	2	22	5	4	34		4
11	43	3	**23**	**4**	**4**	35	6	3
12	**1**	**1**	24	3	2	36		1

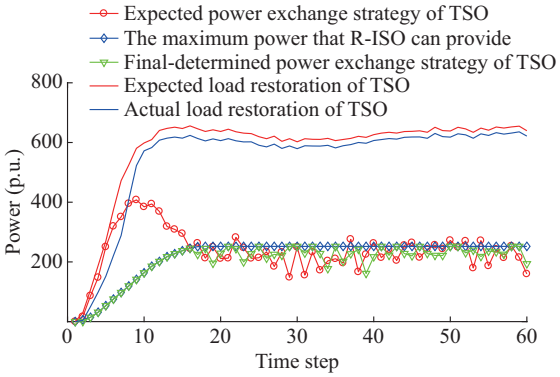

Fig. 6. Coordinated power exchange strategy between R-ISO and TSO.

Regarding the coordinated restoration strategy between the TSO and DSOs, the restoration time steps for 292 TSO and DSO coupling buses are shown in Fig. 7. As shown in Fig. 7, 70.85% of the TSO and DSO coupling buses are restored before the minimum restoration time steps provided by the TSO. However, 29.15% of these buses rely on the TSO for restoration from top to bottom, owing to factors such as insufficient black-start power supply or significant distance between the black-start buses and the TSO and DSO coupling bus.

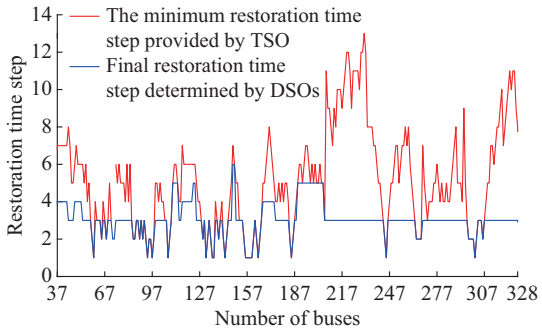

Fig. 7. Restoration time steps for 292 TSO and DSO coupling buses.

To further analyze the coordinated restoration strategy between the TSO and DSOs, DSO 43 is taken as an example, whose coordinated load power restoration strategy is shown in Fig. 8. It can be observed from Fig. 8 that DSO 43 does not restore the load within the first 7 time steps because the TSO does not restore bus 43 until the 7th time step. Subsequently, DSO 43 begins meeting the load power restoration requirements of the TSO to the best of its ability. However, due to the discrete nature of load combinations under each feeder line in practical scenarios, the load power restored by DSO 43 may not precisely match the requirements set by the TSO.

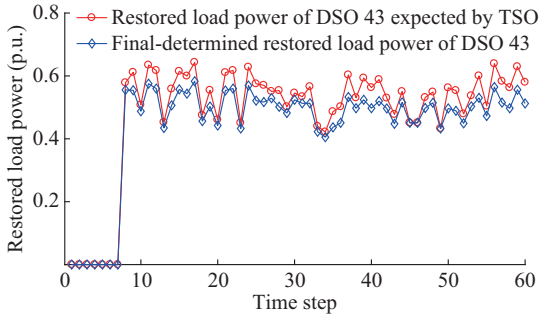

Fig. 8. Coordinated load power restoration strategy between TSO and DSO 43.

D. Comparisons Among Different Restoration Methods

To verify the effectiveness and advantages of the proposed restoration method, it is compared with three other restoration methods: the restoration security risk assessment based spatio-temporal coordinated restoration method for coupled transmission and distribution networks (method A) [6], the restoration security risk assessment based spatio-temporal coordinated restoration method for single power system (method B) [14], and spatio-temporal coordinated restoration method for MVLPSs that does not consider restoration security risk assessment (method C) [15]. The comparison is based on restoration benefits, which are presented in Table II. It can be observed from Table II that the proposed restoration method achieves the highest net restoration benefit among the four methods. Specifically, regarding R-ISO-TSO coordi-

nated restoration, the TSO assists the R-ISO in restoring the network from bottom to top, while the R-ISO provides power generation for the TSO from top to bottom. Regarding TSO-DSO coordinated restoration, the TSO can help DSOs restore the network from top to bottom. Thus, the net restoration benefit of the proposed restoration method is 1.8% higher than that of method A and 1.9% higher than that of method B. Method A enables coordinated restoration between the TSO and DSOs, but the R-ISO and TSO can only be restored independently. Therefore, the net restoration benefit of method A is 0.2% higher than that of method B but 1.8% lower than that of the proposed restoration method. In method B, the R-ISO, TSO, and DSOs can only restore their power generation, network, and load power independently, so its net restoration benefit is the lowest among the four methods. Method C solely focuses on optimizing restoration benefits while disregarding restoration security risks. Consequently, the power re-generation and network restoration benefits of method C exceed those of the proposed restoration method by $\$1.0\times10^6$ and $\$4.2\times10^6$, respectively. However, some transmission lines, such as lines 9-294, 14-285 and 17-263, are situated along the typhoon path. Method C fails to evaluate their restoration security risks and restores these lines at the 10^{th}, 4^{th}, and 4^{th} time steps, incurring restoration security risk control costs of $\$37.4\times10^6$. In contrast, the proposed restoration method assesses the restoration security risks of all transmission lines and schedules their restoration at the 45^{th}, 40^{th}, and 31^{st} time steps, effectively avoiding additional restoration security risk control costs. Consequently, the restoration security risk control cost of the proposed restoration method is $\$11.4\times10^6$ lower than that of method C, resulting in $\$6.2\times10^6$ higher net restoration benefits. In summary, the proposed restoration method optimally coordinates full-stage restoration and security risks across temporal and spatial dimensions, achieving the highest net restoration benefits among all methods.

TABLE II
COMPARISON OF RESTORATION BENEFITS

Method	Power re-generation benefit ($\$10^9$)	Network restoration benefit ($\$10^8$)	Load restoration benefit ($\$10^9$)	Restoration security risk control cost ($\$10^7$)	Net restoration benefit ($\$10^{10}$)
Proposed	6.9603	2.455	4.0391	2.60	1.12188
Method A [6]	6.9446	2.467	3.8516	2.19	1.10210
Method B [14]	6.9446	2.454	3.8374	2.23	1.10051
Method C [15]	6.9603	2.465	4.0433	3.74	1.12126

It should be noted that the proposed restoration method requires a total computational time of 2516 s. This efficiency is achieved by decomposing the overall restoration strategy into independent submodels for the 500 kV, 220 kV, and 110 kV distribution networks, which are then coordinated via a single round of information exchange among the R-ISO, TSO, and DSOs. Compared with existing iterative methods, the proposed restoration method significantly reduces the computational complexity. Given that actual power system restoration processes typically span several hours, a solving time of 2516 s is within a practical range. Moreover, parallel computing, particularly for the independent computations associated with the 110 kV distribution networks, can further accelerate the process, demonstrating both the scalability and practical feasibility of the proposed restoration method.

V. CONCLUSION

A restoration security risk assessment based spatio-temporal coordinated restoration method for MVLPSs is proposed in this paper. The case study based on an actual 379-bus MVLPS in China is conducted to test the effectiveness and advantages of the proposed restoration method, and the following conclusions can be drawn from the simulation.

1) The full-stage restoration strategy for the MVLPSs considering the spatio-temporal coordination among R-ISO, TSO, and DSOs is obtained by the proposed restoration method, which achieves faster black-start, network reconfiguration, and load restoration speeds, leading to higher net restoration benefits compared with existing restoration methods.

2) The restoration security risks of all transmission lines at each time step are assessed accurately and effectively by the proposed spatio-temporal restoration security risk assessment approach, which reduces additional control costs and thus increases the net restoration benefit of the power system compared with the model that solely focuses on optimizing restoration benefits while disregarding restoration security risk.

REFERENCES

[1] C. Chen, H. Liang, X. Zhai *et al*., "Review of restoration technology for renewable-dominated electric power systems," *Energy Conversion and Economics*, vol. 3, no. 5, pp. 287-303, Oct. 2022.
[2] Z. Shi, Y. Xu, D. Xie *et al*., "Optimal coordination of transportable power sources and repair crews for service restoration of distribution networks considering uncertainty of traffic congestion," *Journal of Modern Power Systems and Clean Energy*, vol. 12, no. 1, pp. 189-201, Jan. 2024
[3] Z. Li, Y. Xue, H. Wang *et al*., "Decision support system for adaptive restoration control of transmission system," *Journal of Modern Power Systems and Clean Energy*, vol. 9, no. 4, pp. 870-885, Jul. 2021
[4] N. Ganganath, J. V. Wang, X. Xu *et al*., "Agglomerative clustering-based network partitioning for parallel power system restoration," *IEEE Transactions on Industrial Informatics*, vol. 14, no. 8, pp. 3325-3333, Aug. 2018.
[5] D. Wang, X. Gu, G. Zhou *et al*., "Decision-making optimization of power system extended black-start coordinating unit restoration with load restoration," *International Transactions on Electrical Energy Systems*, vol. 27, no. 9, p. e2367, Sept. 2017.
[6] J. Zhao, Q. Zhang, Z. Liu *et al*., "A distributed black-start optimization method for global transmission and distribution network," *IEEE Transactions on Power Systems*, vol. 36, no. 5, pp. 4471-4481, Sept. 2021.
[7] H. Sekhavatmanesh and R. Cherkaoui, "A multi-step reconfiguration model for active distribution network restoration integrating DG start-

up sequences," *IEEE Transactions on Sustainable Energy*, vol. 11, no. 4, pp. 2879-2888, Oct. 2020.
[8] Y. Wang, Y. Xu, J. Li *et al*., "On the radiality constraints for distribution system restoration and reconfiguration problems," *IEEE Transactions on Power Systems*, vol. 35, no. 4, pp. 3294-3296, Jul. 2020.
[9] D. Xie, Y. Xu, S. Nadarajan *et al*., "Dynamic frequency-constrained load restoration considering multi-phase cold load pickup behaviors," *IEEE Transactions on Power Systems*, vol. 39, no. 1, pp. 107-118, Jan. 2024.
[10] R. R. Nejad and W. Sun, "Distributed load restoration in unbalanced active distribution systems," *IEEE Transactions on Smart Grid*, vol. 10, no. 5, pp. 5759-5769, Sept. 2019.
[11] J. Zhao, H. Wang, Q. Wu *et al*., "Distributed risk-limiting load restoration for wind power penetrated bulk system," *IEEE Transactions on Power Systems*, vol. 35, no. 5, pp. 3516-3528, Sept. 2020.
[12] L. Sun, Z. Lin, Y. Xu *et al*., "Optimal skeleton-network restoration considering generator start-up sequence and load pickup," *IEEE Transactions on Smart Grid*, vol. 10, no. 3, pp. 3174-3185, May 2019.
[13] W. Liu, J. Zhan, C. Y. Chung *et al*., "Availability assessment based case-sensitive power system restoration strategy," *IEEE Transactions on Power Systems*, vol. 35, no. 2, pp. 1432-1445, Mar. 2020.
[14] S. Liu, C. Chen, Y. Jiang *et al*., "Bi-level coordinated power system restoration model considering the support of multiple flexible resources," *IEEE Transactions on Power Systems*, vol. 38, no. 2, pp. 1583-1595, Mar. 2023.
[15] J. Zhao, H. Wang, Y. Liu *et al*., "Coordinated restoration of transmission and distribution system using decentralized scheme," *IEEE Transactions on Power Systems*, vol. 34, no. 5, pp. 3428-3442, Sept. 2019.
[16] J. Zhao, Y. Liu, H. Wang *et al*., "Receding horizon load restoration for coupled transmission and distribution system considering load-source uncertainty," *International Journal of Electrical Power and Energy Systems*, vol. 116, p. 105517, Mar. 2020.
[17] Y. Zhao, Z. Lin, Y. Ding *et al*., "A model predictive control based generator start-up optimization strategy for restoration with microgrids as black-start resources," *IEEE Transactions on Power Systems*, vol. 33, no. 6, pp. 7189-7203, Nov. 2018.
[18] H. Hou, J. Tang, Z. Zhang *et al*., "Stochastic pre-disaster planning and post-disaster restoration to enhance distribution system resilience during typhoons," *Energy Conversion and Economics*, vol. 4, no. 5, pp. 346-363, Oct. 2023.
[19] J. Zhao, H. Wang, Y. Hou *et al*., "Robust distributed coordination of parallel restored subsystems in wind power penetrated transmission system," *IEEE Transactions on Power Systems*, vol. 35, no. 4, pp. 3213-3223, Jul. 2020.
[20] L. Hao, Y. Xue, Z. Li *et al*., "Decision support system for adaptive restoration control of distribution system," *Journal of Modern Power Systems and Clean Energy*, vol. 10, no. 5, pp. 1256-1273, Sept. 2022.
[21] C. Chen, T. Zhang, H. Ma *et al*., "Triple-level full-stage adaptive restoration optimization for coupled transmission and distribution systems considering restoration security risks," *IEEE Transactions on Power Systems*, vol. 39, no. 6, pp. 6833-6848, Nov. 2024.
[22] Y. Wang, Y. Xue, D. Xie *et al*., "Stochastic optimization of medium- and short-term reserve arrangement for preventive and emergency control under typhoon disaster," *Journal of Modern Power Systems and Clean Energy*, vol. 13, no. 1, pp. 190-201, Jan. 2025.
[23] M. Qian, N. Chen, Y. Chen *et al*., "Optimal coordinated dispatching strategy of multi-sources power system with wind, hydro and thermal power based on CVaR in typhoon environment," *Energies*, vol. 14, no. 13, p. 3735, Jul. 2021.
[24] Y. Tang, X. Xu, B. Chen *et al*., "Early warning method of transmission tower considering plastic fatigue damage under typhoon weather," *IEEE Access*, vol. 7, pp. 63983-63991, May 2019.
[25] C. Chen, Y. Li, W. Qiu *et al*., "Cooperative-game-based day-ahead scheduling of local integrated energy systems with shared energy storage," *IEEE Transactions on Sustainable Energy*, vol. 13, no. 4, pp. 1994-2011, Oct. 2022.
[26] C. Chen, Y. Zhu, T. Zhang *et al*., "Two-stage multiple cooperative games-based joint planning for shared energy storage provider and local integrated energy systems," *Energy*, vol. 284, p. 129114, Dec. 2023.
[27] X. Cao, H. Wang, Y. Liu *et al*., "Coordinating self-healing control of bulk power transmission system based on a hierarchical top-down strategy," *International Journal of Electrical Power & Energy Systems*, vol. 90, pp. 147-157, Sept. 2017.

Changming Chen received the B.E. degree in electrical engineering from the College of Electrical Engineering and Automation, Fuzhou University, Fuzhou, China, in 2019, and the Ph.D. degree in electrical engineering from the College of Electrical Engineering, Zhejiang University, Hangzhou, China, in 2024. He is currently a Lecturer (Associate Research Fellow) in the College of Electrical Engineering and Automation, Fuzhou University, Fuzhou, China. His research interests include power system restoration, shared energy storage, and integrated energy system optimization.

Yunchu Wang received the B.E. degree in electrical engineering from Zhejiang University, Hangzhou, China, in 2020. She is currently pursuing the Ph.D. degree with the College of Electrical Engineering, Zhejiang University. Her research interests include power system economics and optimization, and demand response.

Shunjiang Yu received the B.E. degree from China Agricultural University, Beijing, China, in 2020, and the M.S. degree from Xi'an Jiaotong University, Xi'an, China, in 2023, both in electrical engineering. He is currently pursuing the Ph.D. degree with the College of Electrical Engineering, Zhejiang University, Hangzhou, China. His research interests include optimal planning and scheduling of integrated electricity and heat systems.

Bing Chen received the M.S. degree from Guangxi University, Nanning, China, in 2005, and the Ph.D. degree from South China University of Technology, Guangzhou, China, in 2008. He currently works with State Grid Jiangsu Electric Power Co., Ltd., Nanjing, China. His research interests include power quality, high-voltage direct current (HVDC), and power electronics applied in power system.

Zikang Shen received the B.E. degree in electrical engineering from the School of Electrical and Information Engineering, Tianjin University, Tianjin, China, in 2022. He is currently pursuing the Ph.D. degree in electrical engineering with the College of Electrical Engineering, Zhejiang University, Hangzhou, China. His research interests include electricity market, and power system planning and optimal dispatch.

Ze Li received the B.E. and Ph.D. degrees in electrical engineering from Southeast University, Nanjing, China, in 2014 and 2021, respectively. He is currently a Senior Engineer of State Grid Electric Power Research Institute (NARI Group Corporation), Nanjing, China. His research interests include power system security analysis and control.

Hongtao Wang received the B.S. and M.S. degrees in electrical engineering from Shandong Polytechnic University, Jinan, China, in 1995 and 1998, respectively, and the Ph.D. degree in electrical engineering from Shandong University, Jinan, China, in 2005. He was a Postdoctoral Researcher with the Department of Computer Science, Shandong University. From 2005 to 2010, he was an Associate Professor with the School of Electrical Engineering, Shandong University, where he has been a Professor since 2010. His research interests include power system analysis and control, and smart grid.

Zhenzhi Lin received the Ph.D. degree in electrical engineering from South China University of Technology, Guangzhou, China, in 2008. He was a Research Assistant in the Department of Electrical Engineering at The Hong Kong Polytechnic University, Hong Kong, China, from 2007 to 2008, a Research Scholar in the Department of Electrical Engineering and Computer Science at the University of Tennessee, Knoxville, USA, from 2010 to 2011, and a Research Associate in College of Engineering and Computing Sciences at Durham University, Durham, U.K., from 2013 to 2014. He is currently a Professor in the College of Electrical Engineering, Zhejiang University, Hangzhou, China. His research interests include power system wide-area monitoring and control, controlled islanding and power system restoration, and data mining in power systems.